Eur. Phys. J. D (2014) 68: 151
DOI: 10.1140/epjd/e2014-40699-0

THE EUROPEAN PHYSICAL JOURNAL D

Regular Article

Electron impact fragmentation of thymine: partial ionization cross sections for positive fragments*

Peter J.M. van der Burgt[a], Francis Mahon, Gerard Barrett, and Marcin L. Gradziel

Department of Experimental Physics, National University of Ireland Maynooth, Maynooth, Co. Kildare, Ireland

Received 8 November 2013 / Received in final form 2 April 2014
Published online 23 June 2014 – © EDP Sciences, Società Italiana di Fisica, Springer-Verlag 2014

Abstract. We have measured mass spectra for positive ions for low-energy electron impact on thymine using a reflectron time-of-flight mass spectrometer. Using computer controlled data acquisition, mass spectra have been acquired for electron impact energies up to 100 eV in steps of 0.5 eV. Ion yield curves for most of the fragment ions have been determined by fitting groups of adjacent peaks in the mass spectra with sequences of normalized Gaussians. The ion yield curves have been normalized by comparing the sum of the ion yields to the average of calculated total ionization cross sections. Appearance energies have been determined. The nearly equal appearance energies of 83 u and 55 u observed in the present work strongly indicate that near threshold the 55 u ion is formed directly by the breakage of two bonds in the ring, rather than from a successive loss of HNCO and CO from the parent ion. Likewise 54 u is not formed by CO loss from 82 u. The appearance energies are in a number of cases consistent with the loss of one or more hydrogen atoms from a heavier fragment, but 70 u is not formed by hydrogen loss from 71 u.

1 Introduction

In recent years many studies of electron collisions with molecules have focused on biomolecules such as the nucleobases in the gas phase (for reviews see [1–5]). The purpose of this article is to present new results for low-energy electron impact to thymine in the gas phase leading to the formation of positively charged fragments. Several groups have already looked at mass spectra of thymine, but in this article we present ionization cross sections for most of the positively charged fragments. We have normalized the yield curves of the fragment ions by comparing the total ion yield to the total ionization cross section of thymine obtained from theoretical calculations. The aim of this article is to present these results, which provide new information about the appearance energies of the positive fragments, the fragmentation pathways initiated by electron impact, and the ionization cross sections for the production of these ions.

Thymine has been the focus of a number of collisions studies involving electron, photon and ion impact. Mass spectrometry following 20 eV and 70 eV electron impact on thymine, ^{14}C2-thymine and thymine-d$_3$-6-d has been performed by Rice et al. [6], Ulrich et al. [7], and Imhoff et al. [8]. Their results will be compared with our results later in this paper.

Electron energy-loss spectroscopy has been used by Abouaf et al. [9] to study electronic and vibrational excitation of thymine molecules. Dal Cappello et al. [10,11] present theoretical and experimental triply differential cross sections for the ionization of thymine by 250 eV electrons and positrons and compare these with first and second Born calculations.

Dissociative electron attachment (DEA) has been studied by Huels et al. [12], Denifl et al. [13,14] and Abouaf and Dunet [15]. The most comprehensive study [14] identifies 9 different reaction channels for the formation of different negative ions. DEA of partly deuterated thymine and methylated thymine [16–21] have shown that resonances observed in the yields of the negative fragment ions are associated with very specific bond breakages in the thymine molecule.

A comprehensive study of vibrational Feshbach resonances in DEA of thymine has been performed by Burrow et al. [22]. Other theoretical work includes a study of hydrogen loss via DEA [23], an R-matrix study of elastic and inelastic electron collisions with thymine [24], and the application of density functional theory to radical cations of thymine [25].

Jochims et al. [26] have used synchrotron radiation for photo-ion mass spectrometry of thymine in the 6−22 eV photon energy range. Itälä et al. [27] have studied soft X-ray (330 eV) induced fragmentation processes of thymine using a photoelectron-photoion-photoion coincidence technique.

* Contribution to the Topical Issue "Electron and Positron Induced Processes", edited by Michael Brunger, Radu Campeanu, Masamitsu Hoshino, Oddur Ingólfsson, Paulo Limão-Vieira, Nigel Mason, Yasuyuki Nagashima and Hajime Tanuma.

[a] e-mail: peter.vanderburgt@nuim.ie

A variety of studies of ions colliding with thymine in the gas phase have been performed. Schlathölter and coworkers [28–32] have used time-of-flight mass spectrometry to study $C^{q+}(q = 1-6; 4\,keV/u)$ and $Xe^{q+}(q = 5-25; 0.5\,MeV)$ collisions with thymine. Tabet et al. [33] present results for 80 keV proton impact with separation of direct ionization and electron capture.

Very recently there has been an increased interest in collisions of DNA base clusters and DNA bases embedded in clusters. Kim et al. [34] have determined ionization potentials of hydrated thymine under electron impact. Kim et al. [35] (different group) have studied UV photofragmentation of thymine clusters. Kagawa et al. [36] have studied fragmentation of hydrated thymine by UV laser pulses at 266 nm. Schlathölter et al. [37] have applied coincidence time-of-flight spectrometry in collisions of keV ions with thymine clusters. Zappa et al. [38] have studied electron impact ionization of thymine clusters embedded in superfluid helium droplets.

The present paper focuses exclusively on collisions with isolated thymine molecules. In the following sections we discuss our experimental set-up, the data acquisition, and the methods used for analysis of the data. We then present the results, compare these with other research, in particular electron and photon impact mass spectrometry, and discuss possible reaction mechanisms.

2 Experiment

The experimental set-up consists of a small oven producing an effusive beam of thymine molecules, a pulsed electron beam, and a reflectron time-of-flight mass spectrometer. An overview of the experiment can be found in reference [39]. The pulsed valve used in reference [39] for the generation of clusters has been replaced by the oven.

The thymine beam is generated by resistively heating the oven containing thymine powder (from Sigma Aldrich, 99% purity) to a temperature of 180 °C (453 K). The molecular beam effuses from a capillary (0.5 mm diameter and 4.5 mm length), and passes through a skimmer (1.2 mm diameter) into the collision chamber, where the beam is crossed by the electron beam. The alignment of the oven, skimmer and electron gun is ensured by the mounting of all these components on the top hat that separates the source chamber containing the oven from the collision chamber.

The electron beam has an energy resolution of about 0.8 FWHM and is pulsed at a rate of 8 kHz with a 1.0 μs pulse width. Positively charged fragments are extracted into the mass spectrometer 0.8 μs after the electron pulse. A delay generator (Stanford Research Systems DG535) is used to synchronize the pulsing of the electron gun, the ion extraction voltage, and the start of the multichannel scaler (FastComtec 7886S).

A LabVIEW program has been developed to control the data acquisition. The program steps through all electron impact energies by incrementing the electron impact energy by 0.5 eV via a programmable power supply, reading the mass spectrum acquired by the multichannel scaler, and adding it to the data already accumulated in the appropriate place in a two-dimensional array. After each cycle through all electron impact energies, which takes about two hours, the full data set is saved. The full data set consists of a two-dimensional array of ion yield as a function of time-of-flight and as a function of electron impact energy. The data set used for extracting the ion yield curves presented in this paper consists of 14 cycles.

Several tests have been done to make sure that the ion yield curves could reliably be collected from the full data set and be normalized to the total ionization cross section. The optimization of the electron gun was done in pulsed mode by maximizing the current on the Faraday cup and ensuring that the current was independent of electron impact energy. In this way an electron beam was produced with a total current that was constant down to 15 eV and dropping to 60% at 8 eV. Several tests have been done in which one of the voltages in the mass spectrometer was varied and the yields of the most prominent peaks in the mass spectrum were recorded. In this way voltages could be selected such that the mass spectrometer was optimized simultaneously for the detection of ions of different masses in the range 12−126 u. Two mass spectra acquired at an electron energy of 100 eV for an equal number of electron pulses at pulse rates of 8 kHz and 400 Hz were observed to be identical apart from minor statistical fluctuations. By examining mass spectra obtained after successive cycles, it has been verified that that there were no undesired effects during the collection of the data.

3 Data analysis

3.1 Ion yield curves

The mass resolution of the mass spectrometer is $\Delta m/m = 0.0045$ at 126 u, and above 20 u adjacent peaks in the mass spectra are not fully separated. Ion yields have been determined by fitting adjacent peaks with sequences of normalized Gaussians. Ion yield curves have been obtained by using a LabVIEW program that fits 200 mass spectra in succession for all electron impact energies and for each group of peaks.

As the electron impact energy reached values close to the appearances energies for the peaks, problems with convergence of the fits were encountered. For this reason most fits were repeated in a region of low electron energies using a reduced number of peaks and/or a fixed value of the peak width set to the average of the fitted widths at higher energies. The data points close to threshold in the ion yield curves were obtained from these low-energy fits. In all cases it was verified that there was a region of overlap in which the low-energy fits produced close to the same values for the fitted parameters as the fits at higher electron energies.

During our experiments with thymine we have observed a gradual depletion of the intensity of the thymine beam, which was not due to the oven running empty or the capillary becoming blocked. We are not sure of the cause

of this, but this has not been observed in experiments with the other nucleobases. A small correction factor was applied to all ion yield curves obtained from the dataset (ranging from 1 at 0 eV to 1.0488 at 100 eV).

We have not been able to fully eliminate the presence of water in our vacuum system and ion yield curves of the 1 u and 16−18 u fragments are not presented. We see no indication of a thymine-water dimer (144 u) in the mass spectra, so the presence of water has had no effect on the data for thymine. The 17 u and 18 u ion yield curves obtained from the fitting procedure have been used for calibration of the incident electron energy by comparison with the recommended ionization cross sections for the production of H_2O^+ and OH^+ in Itikawa and Mason (Tab. 11 in [40]) in the range 10−40 eV. The estimated error in the calibration is ±0.2 eV.

3.2 Appearance energies

Appearance energies (onsets) have been determined by fitting an onset function convoluted with a Gaussian (see Denifl et al. [41] and references therein) to each of the ion yield curves using LabVIEW. For a single onset at E_0, the formula used is:

$$P(E) = \int_{-\infty}^{\infty} f(\varepsilon) g(E-\varepsilon) d\varepsilon + b$$

with

$$f(\varepsilon) = 0 \qquad \text{if } \varepsilon \leqslant E_0$$
$$f(\varepsilon) = c(\varepsilon - E_0)^p \qquad \text{if } \varepsilon > E_0$$

and

$$g(\varepsilon) = \frac{1}{\sigma\sqrt{\pi}} \exp\left(-\varepsilon^2/\sigma^2\right)$$

in which the electron beam width is set at $\sigma = 0.8$ eV, and E_0, b, c and p are the fitted parameters. In the case of two or three onsets, one or two extra terms are added to the function $f(\varepsilon)$. The convolution integral is evaluated using a 9-point Gauss-Hermite quadrature.

3.3 Normalization of the data

Assuming that the ion collection and detection efficiency of the mass spectrometer is mass independent, all ion yield curves extracted from the data set are on the same relative scale, and the sum of the curves can be normalized to the total ionization cross section. We have obtained two curves for the total ionization cross section as a function of electron impact energy. Figure 1 compares both curves with other experimental [42] and theoretical data [43–46].

The first curve is the sum of all the ion yield curves obtained from the fitting procedure. The normalization factor is 3.36×10^{-25}, which normalizes this curve at 70 eV to the average of the theoretical cross sections presented in Figure 1. This normalization provides good overall agreement with the shapes of the theoretical curves in the range

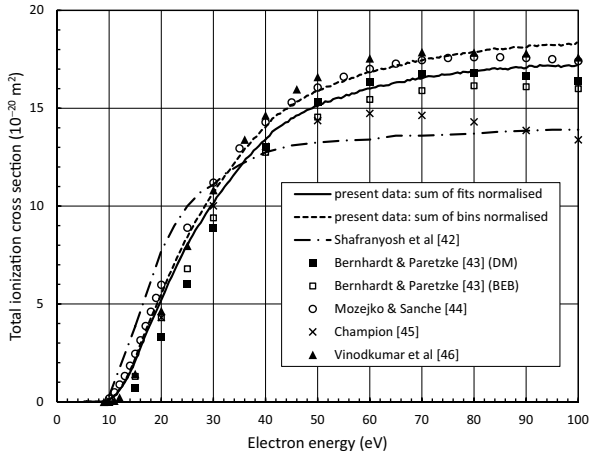

Fig. 1. Total ionization cross sections for electron impact on thymine. The lines indicate experimental results; the symbols are theoretical results. A normalization factor of 3.36×10^{-25} has been applied to both the sum of the fits and the sum of the bins. This factor normalizes the sum of the fits at 70 eV to the average of the theoretical cross sections in the figure.

9−100 eV. Because this curve does not include the production of the 1 u, and the 16−18 u fragments from electron impact of thymine, it slightly underestimates the total ionization cross section.

The second curve is simply the sum of all the counts collected in the mass spectra as a function of electron impact, with the exclusion of 1 u, 16−18 u, and 32 u. This is a small overestimate of the total ionization cross section, because it contains background signals under and in between the thymine peaks. We have used the same normalization factor for the second curve. There is only a small difference between both curves, and the shape of the curves is in very good agreement with four of the theoretical calculations. Based on this agreement, we have applied the same normalization factor to the ion yield curves of each of the fragments to obtain partial ionization cross sections

4 Results and discussion

4.1 Total ionization cross section

Looking again at Figure 1, it is seen that there is a significant difference in the shapes of the curves total ionization cross sections obtained by us and by Shafranyosh et al. [42]. They were able to put their cross sections on an absolute scale by measuring the density of molecules in the beam by condensing their thymine beam onto a plate held at liquid nitrogen temperature. Because we have normalized our data to the theory, we cannot comment on the disagreement between the total ionization cross sections obtained by Shafranyosh et al. [42] and by the various theories. However, the shape of our curve is is in better agreement with four of the calculated cross sections than the curve of Shafranyosh et al. [42].

Five theoretical cross sections [43–46] are included in Figure 1. Calculations by Huo et al. [47] and Peudon

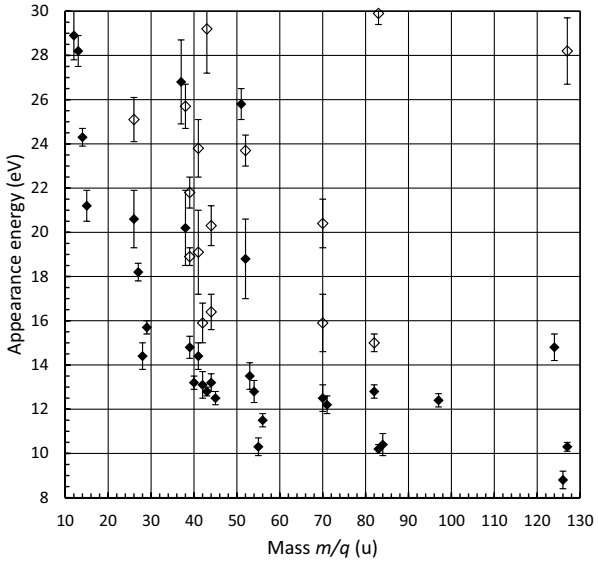

Fig. 2. Appearance energies for positive fragment ions of thymine. For each fragment, the lowest onset is shown as a solid diamond, and higher onsets are shown as open diamonds. Four onsets above 30 eV are listed in the text.

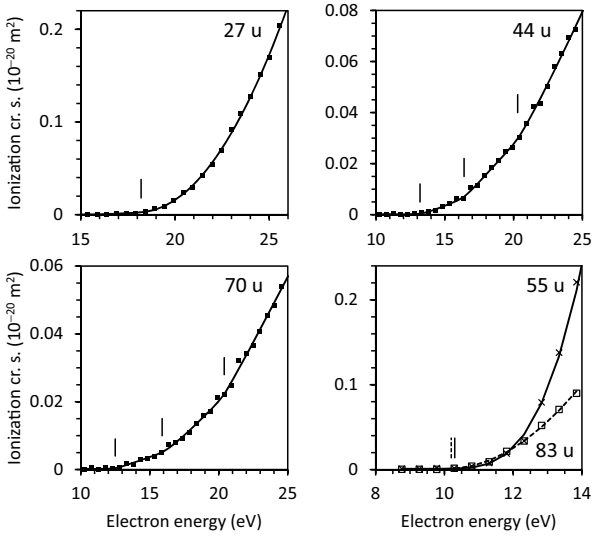

Fig. 3. Partial ionization cross sections of five selected thymine fragments. The appearance energies, second and third onsets, and fitted onset functions are also shown. 55 u and 83 u have nearly the same appearance energy.

et al. [48] are not shown in the figure; for comparisons see Figure 4 in [46]. The theoretical curves are in good agreement with each other in the range 9−100 eV. Compared to the other calculations, the curve from Champion [45] drops more rapidly above 60 eV. Champion [45] comments that the shapes of the theoretical curves from 10 to 1000 eV are very similar, but that there are differences in the heights and the positions of the maxima.

4.2 Appearance energies

Figure 2 shows the appearance energies obtained for each of the thymine fragments. The errors are based on the fits only, and do not incorporate the error in the energy calibration. Four onsets above 30 eV are not shown in the graph: 12 u: 43.7 ± 2.7 eV, 25 u: 32.5 ± 1.1 eV, 37 u: 33.3 ± 1.0 eV, and 51 u: 33.4 ± 0.7 eV. Figure 3 shows partial ionization cross sections of five selected fragments, their appearance energies, and fitted onset functions.

Our appearance energy for the parent ion, 8.8 ± 0.4 eV, is in good agreement with other measurements of the ionization energies of thymine, listed in Table 4 of reference [26].

Table 1 compares the appearance energies observed for electron impact in the present work with those obtained for photon impact by Jochims et al. [26]. Whereas some of the appearance energies are in reasonable or good agreement, others are clearly different. Several of our ion yield curves rise very rapidly just above threshold, requiring high values of p in the fits (e.g. $p = 1.71 \pm 0.11$ for 126 u, $p = 1.9 \pm 0.2$ for 83 u and $p = 3.0 \pm 0.4$ for 55 u). The best values of the fitted parameters and their estimated errors are therefore based on the selections of data points above threshold that are included in the fits.

Table 1. Comparison of appearance energies for electron impact and for photon impact.

	Present data	Jochims et al. [26]
126 u	8.8 ± 0.4	8.82 ± 0.03
83 u	10.2 ± 0.2	10.70 ± 0.05
82 u	12.8 ± 0.3	13.20 ± 0.05
55 u	10.3 ± 0.4	11.7 ± 0.1
54 u	12.8 ± 0.5	≈12.9
43 u	12.8 ± 0.2	11.9 ± 0.1
39 u	14.8 ± 0.5	14.4 ± 0.1
28 u	14.4 ± 0.6	13.6 ± 0.1

Notably the appearance energies for the 83 u and 55 u fragments are lower than those reported by Jochims et al. [26]. Figure 3 (bottom-right) shows the ion yield curves for both fragments in the 4 eV region above threshold. Between 10.8 and 12.3 eV the ion yields for both fragments have very similar values. In previous work ([6,8,26]) it is generally considered that the 83 u and 55 u fragments are resulting from a successive loss of HNCO and CO from the parent ion. However, the nearly equal onsets observed in the present work strongly suggest that near threshold the 55 u ion is formed directly by the breakage of two bonds in the ring. This will be discussed further in Section 4.3.5.

The higher appearance energies observed for 82 u compared to 83 u, and for 54 u compared to 55 u, are both consistent with the loss of an additional hydrogen atom. Other sequences of progressively higher onsets indicate the formation of smaller fragments by successive loss of hydrogen atoms: 53-52-51 u, 40-39-38-37 u, 28-27-26 u and 15-14-13 u.

In several of the ion yield curves we observe second and (occasionally) third onsets. This is not unexpected for the smaller fragments, because multiple fragmentations may be possible for the formation of these, but it is difficult to draw specific conclusions with regard to possible

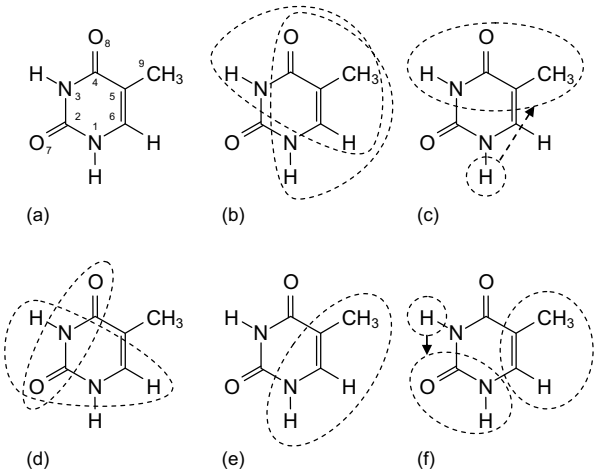

Fig. 4. (a) Structure of the thymine molecule, (b)–(e) possible dissociation processes of the core-ionized thymine molecule. The encircled regions show possible assignments of the observed positive ions (see text for more details): (b) 83 u, (c) 71 u, (d) 70 u, (e) 55 u, and (f) 44 u (left) and 40 u (right).

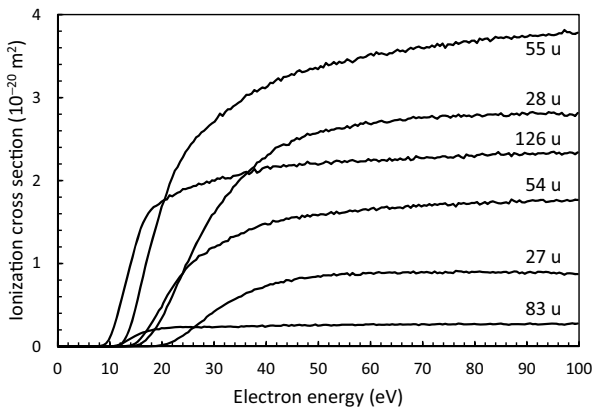

Fig. 5. Partial ionization cross sections of the 5 most abundant fragments of thymine. Because of its low appearance energy, the partial ionization cross section of 83 u is also shown.

fragmentation processes. Contrary to cytosine [49], the 13−15 u fragments of thymine do not show second onsets, but the ion yield curves of these fragments have poor statistics.

4.3 Partial ionization cross sections and fragmentation processes

In the following paragraphs we consider possible fragmentation processes based on the data we have obtained, and on the results of earlier research. We have grouped the peaks such that the group number is the number of C, N, and O atoms in the fragment. Prominent fragmentations are illustrated in Figure 4, which also shows the structure of the thymine molecule. Lists of possible configurations of each of the fragment ions can be found in Table 3 of Jochims et al. [26] and Table 4 of Tabet et al. [33].

Ion yield curves for the five most abundant fragments are presented in Figure 5. For comparison the ion yield curve of 83 u is also shown. Most of the other ion yield curves are presented in Figures 6–8, and will be discussed below. A full set of ion yield curves can be obtained from the authors.

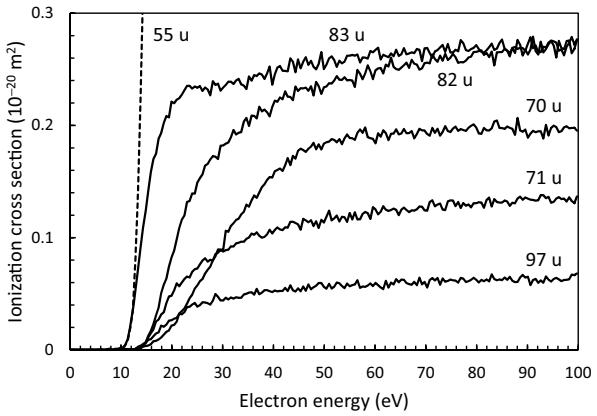

Fig. 6. Partial ionization cross sections of the 97 u, 83 u, 82 u, 71 u and 70 u fragments of thymine. Part of the partial ionization cross section of 55 u (dashed line) is also shown for comparison.

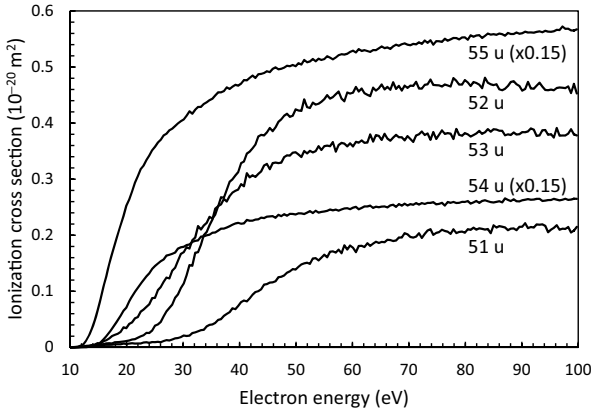

Fig. 7. Partial ionization cross sections of the 51−55 u fragments of thymine.

Thymine can occur in different tautomeric forms (see e.g. [50–52]), but spectroscopic studies show that at the temperature used in our oven only one tautomer is present (see discussion in Ref. [26]). Measurements of electron ionization of cytosine [49] have shown that several groups of fragments have ion yield curves with nearly the same shape, pointing to the relevance of tautomerization in the fragmentation of cytosine, but we do not see such similarities in the ion yield curves of thymine. However, the formation of the 71 u fragment likely involves a bond rearrangement with a hydrogen atom (see discussion below).

4.3.1 Group 9 (124, 126, 127 u)

As discussed above, 126 u has an appearance energy of 8.8 ± 0.4 eV, in good agreement with other research (see Tab. 4 in [26]). This is the lowest onset observed.

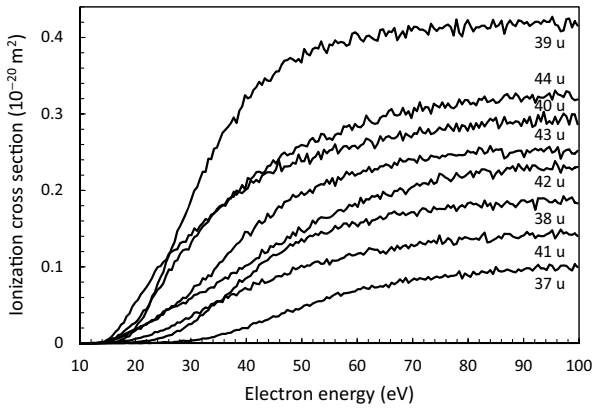

Fig. 8. Partial ionization cross sections of the 37−44 u fragments of thymine.

The presence of 127 u (10% of 126 u at 100 eV) could be due to an isotope contribution and/or protonated thymine. Protonated thymine could possibly be the formed in the decay of thymine dimmers, which would explain the somewhat higher appearance energy of 127 u, but we do not see any indication of fragments in the range 128−166 u (we did not extend our time-of-flight range to higher masses). Because the 127 u peak is weak and in the tail of the very prominent 126 u peak, the fitted area of this peak may be less reliable, and the 127 u ion yield curve is not shown in this paper.

Given that 55 u and 28 u are the most prominent fragments of thymine, 56 u and 29 u could mostly be due to the fragmentation of 127 u. Similar to 83 u and 55 u, the ion yield curves of 84 u and 56 u have very low appearance energies. 45 u may also be a fragment of 127 u. We will not discuss these fragments in the remained of this paper, but the appearance energies for these fragments are included in Figure 2.

There is a very weak peak at 124 u, with an appearance energy which is consistent with the loss of two hydrogen atoms. No other peaks are observed in this group. This is in contrast to dissociative electron attachment, in which various fragmentations leading to 124 u and 125 u negative ions have been observed [13–16].

4.3.2 Group 7 (97 u)

We observe the weak presence of 97 u in our mass spectra. This fragment is not discussed in references [6,8], although it is present in the 70 eV mass spectrum in reference [6]. The mass spectrum of ^{14}C2-thymine [7] shows this fragment at 99 u, indicating that it contains the C2 atom. Jochims et al. [26] suggest that this fragment is possibly $C_4H_3NO_2^+$, resulting from the loss of NH_2CH, i.e. the simultaneous loss of the HCNH group and a single hydrogen atom. Another possibility is the simultaneous loss of the CO group containing the C4 atom and a single hydrogen atom. Denifl et al. [14] identify this as the configuration of 97 u observed in dissociative electron attachment. The ion yield curve of 97 u is shown in Figure 6. A number of smaller fragments (54 u, 55 u, 71 u, 83 u) have lower appearance energies than 97 u, which shows that these fragments are not produced by further fragmentation of 97 u.

4.3.3 Group 6 (82, 83 u)

Various authors have identified the loss of HNCO as the pathway leading to the 83 u fragment. There are three possible configurations for the resulting 83 u fragment, but calculations by Improta et al. [25] of possible minimum energy structures and relative stabilities of $C_4H_5NO^+$ isomers indicate that the $[OC\text{-}C_3H_4\text{-}NH]^+$ structure resulting from the N1-C2 and N3-C4 bond breaks is the most likely.

Imhoff et al. [8] have observed the 83 u fragment to shift to 87 u in the case of electron impact fragmentation of thymine-d_3-6-d, but this does not rule out any of the three possible configurations (this does rule out simultaneous HNCH + CH_3 loss). However, the mass spectrum of ^{14}C2-thymine [7] shows no shifts of the 82 u and 83 u peaks, so the structure resulting from the C2-N3 and C4-C5 bonds is ruled out. The possible fragment ion configurations are shown in Figure 4b.

The 82 u fragment could be produced by H loss from 83 u, consistent with the higher onsets observed in [26] and in the present work, see Table 1. The loss of the CH_3 or the NH group from 97 u (if formed by CO and H loss) is ruled out by the fact that the 82 u peak does not shift in the mass spectrum of ^{14}C2-thymine. The ion yield curves for these fragments are shown in Figure 6. At higher electron energies the formations of 82 u and 83 u become equally likely.

4.3.4 Group 5 (70, 71 u)

70 u and 71 u are clearly present in our mass spectra. At higher electron energies, the formation of 70 u is more likely than 71 u (see Fig. 6). The ion yield curve of 70 u shows three onsets (Fig. 3, bottom left), whereas only one onset has been identified for 71 u.

70 u and 71 u are also visible in the mass spectra in references [6–8], and are reported in reference [26]. The peaks shift to 71 u and 72 u in the mass spectrum of ^{14}C2-thymine [7], which indicates that the 70 u fragment contains the C2 atom, whereas the 71 u fragment does not. We consider four possible combinations of two bond breaks in the ring, each resulting in a fragment with 5 C, N, and O atoms.

Breakage of the N1-C6 and N3-C4 bonds would result in $C_4H_4O^+$ (68 u) with the loss of CH_2N_2O (58 u), but 68 u and also 58 u are absent in our mass spectra, so pathways producing stable ionized fragments of either of these masses do not exist. In contrast to this, 68 u has been observed in DEA [14].

Breakage of the N1-C2 and C4-C5 bonds would lead to $OCNHCO^+$ (71 u, containing the C2 atom), with the loss of C_3H_5N (55 u). Loss of an additional hydrogen atom

could lead to $OCNCO^+$, which is a possible pathway for the formation of 70 u. This pathway has been suggested by Ulrich et al. [7].

Breakage of the N3-C4 and C5-C6 bonds would lead to $C_2H_3N_2O^+$ (71 u, also containing the C2 atom), with the loss of C_3H_3O (55 u). Loss of an additional hydrogen atom (from 3 possible locations) would yield $C_2H_2N_2O^+$ which is another possible pathway for the formation of 70 u. Both these fragmentations are illustrated in Figure 4d. This pathway, followed by a N3-C6 bond formation, leading to a structure of the 1,2,5-oxadiazole cation, has been suggested by Jochims et al. [26].

Both pathways just discussed are ruled out for 71 u, because the 71 u fragment does not contain the C2 atom. Jochims et al. [26] incorrectly assign 71 u to $OCNHCO^+$. Denifl et al. [14] in DEA assign 71 u to $C_2H_3N_2O^-$, which is still a possibility if DEA follows different fragmentation pathways.

The only possibility left is that the 71 u positive ion is formed by breakage of the C2-N3 and C5-C6 bonds, followed by a bond rearrangement where one hydrogen atoms from the other fragment attaches to the C5 atom, resulting in $C_3H_4NO^+$. This is illustrated in Figure 4c. The slightly higher appearance energy of 70 u could be consistent with this.

4.3.5 Group 4 (51–56 u)

In this group we observe clear peaks from 51 u to 56 u. The partial ionization cross sections for 51−55 u have very different shapes (Fig. 7). At electron energies above 20 eV the 55 u fragment has the highest yield in the mass spectrum. Purely based on the geometry of the parent molecule, several configurations could be proposed for the 55 u ion, however, based on the observed shift of the 55 u peak to 59 u in the mass spectrum of thymine-d_3-6-d, Imhoff et al. [8] assign 55 u to $HNC_3H_4^+$. This is consistent with the mass spectrum of ^{14}C2-thymine [7], which has 55 u as the highest peak in this group, indicating that this ion does not contain the C2 atom.

In previous work [6,8,26] it is generally considered that the 83 u and 55 u fragments are resulting from a successive loss of HNCO (N1-C2 and N3-C4 bond breaks) and CO (C4-C5 bond break) from the parent ion. However, the essentially equal onsets observed in the present work strongly suggest that near threshold the 55 u ion is formed directly by the breakage of the N1-C2 and C4-C5 bonds. This is illustrated in Figure 4e. This does not exclude the possibility of a successive loss of HNCO and CO at higher electron impact energies.

The 54 u ion has the second-highest yield in this group. The higher onset for 54 u is consistent with the loss of a hydrogen atom from 55 u. For thymine-d_3-6-d, Imhoff et al. [8] observe two peaks at 57 u and 58 u, also consistent with the loss of a single H or D atom. The appearance energies of 82 u and 54 u obtained in this work are equal, which implies that near threshold 54 u is not formed by CO loss from 82 u. However, combined CO and H loss from 83 u would still be a possibility. 54 u has also been observed in DEA [14].

For the remaining peaks it is difficult to draw any conclusions from our measurements. The higher onsets of 52 u and 51 u are consistent with loss of one or more hydrogen atoms from the higher masses. It is not possible to provide definitive assignments for the 51−53 u fragments.

4.3.6 Group 3 (37–44 u)

The progressively increasing onsets for 40 u, 39 u, 38 u, and 37 u are consistent with the loss of one or more hydrogen atoms. The relative intensities of these peaks do not change much in the spectrum of ^{14}C2-thymine [7] indicating that these fragments do not contain the C2 atom. However, the peaks in this group shift to higher mass in the mass spectrum of thymine-d_3-6-d [8], indicating that these fragments contain one or more D atoms. This excludes the assignment of 40 u to either $C_2H_2N^+$ or C_2O^+.

As in previous work [8], 40 u is assigned to $C_3H_4^+$, illustrated in Figure 4f, with 39 u, 38 u, and 37 u formed by loss of one or more hydrogen atoms. The ion yield curves show that above 26 eV 39 u has the highest yield in this group. 40 u has an appearance energy that is 2.9 eV higher than that of 55 u, so this ion could be formed by HN loss from $HNC_3H_4^+$. Imhoff et al. [8] suggest that the peak at 40 u may be partly due to NCN^+, but this is contradicted by the mass spectrum of ^{14}C2-thymine [7] which indicates that 40 u does not contain the C2 atom.

Looking at the 41−44 u peaks, there seem to be some shifts to higher mass in the mass spectra of ^{14}C2-thymine [7] and thymine-d_3-6-d [8]. We observe nearly the same appearance energies for 40 u, 42 u, 43 u, and 44 u (12.8−13.2 eV), whereas the appearance energy of 41 u is about 1.4 eV higher. The ion yield curves in this group are quite similar, and 44 u has the highest yield (see Fig. 8). This indicates that there may be different fragmentation processes leading to 42 u, 43 u, and 44 u, but that the weak peak at 41 u is due to hydrogen loss from 42 u.

In the absence of any bond rearrangements and loss of individual hydrogen atoms, the only possible assignment of 43 u is to $HNCO^+$ ([6,8,26]). There are three possible combinations of breakage of two bonds in the ring that could lead to this configuration. The appearance energy of 43 u shows that this fragment could be formed by successive fragmentation via bigger fragments (83 u, 71 u, 70 u). 43 u is also a prominent fragment in soft X-ray induced fragmentation of thymine [27].

Imhoff et al. [8] have suggested that 44 u may be assigned to CH_2NO^+ formed by the oxygen atom in the $HNCO^+$ fragment abstracting a hydrogen atom from either the CH_3 group or the NH group. This is illustrated in Figure 4f.

42 u has a slightly higher appearance energy than 43 u, indicating that this fragment could be formed by hydrogen loss from 43 u. Another possibility is CNO^+ formed by loss of CO from $OCNCO^+$ (70 u). An unlikely possibility is $CH_2N_2^+$ formed by the breaking of two diagonal bonds

in the parent molecule producing $CH_2N_2O^+$ (58 u, not observed), followed by the loss of the O atom producing $CH_2N_2^+$ Loss of a hydrogen atom would then produce CHN_2^+ (41 u). 42 u has also been observed in DEA [14].

5 Conclusion

Although selective bond breaking by electron impact leading to positive fragments is not as clearly visible as in dissociative electron attachment (DEA), the comparison of the mass spectra of thymine, ^{14}C2-thymine [7] and thymine-methyl-d_3-6-d [8] rules out a number of possible fragmentations, allows the identification of the structure of some fragments, and clearly shows that also in the production of positively charged fragments selective dissociation pathways are preferred.

The appearance energies determined in the present work reduce the number of possible successive fragmentations leading to smaller fragments. The appearance energies are in a number of cases consistent with the loss of one or more hydrogen atoms from a heavier fragment (83-82 u, 55-54 u, 53-52-51 u, 40-39-38-37 u, 28-27-26 u and 15-14-13 u).

In previous papers it has been suggested that the 83 u and 55 u fragments are resulting from a successive loss of HNCO and CO from the parent ion. However, the nearly equal appearance energies of these fragments observed in the present work strongly indicate that near threshold the 55 u ion is formed directly by the breakage of two bonds in the ring, and that 83 u and 55 u may be formed via different fragmentation pathways. The equal appearance energies of 82 u and 54 u indicate that near threshold 54 u is not formed by CO loss from 82 u.

The mass spectrum of ^{14}C2-thymine [7] indicates that the 70 u fragment contains the C2 atom, whereas the 71 u fragment does not. This restricts the possible configurations of both fragments, shows that 70 u is not formed by hydrogen loss from 71 u, and implies that 71 must be formed via a double bond break in the ring, followed by a bond rearrangement with a hydrogen atom, possibly related to tautomerization in the fragmentation.

The authors gratefully acknowledge financial support for scientific visits received from the Nano-IBCT project (COST Action MP1002) and the ITS-LEIF project (FP6 Grant No. RII3-026015), both funded by the European Union. Part of the equipment used in this experiment was funded by Enterprise Ireland. The authors also wish to acknowledge Mr. David Watson for his contributions to the mechanical design of the apparatus and to Mr. Pat Seery for his contributions to the electronics equipment.

References

1. H. Hotop, M.-W. Ruf, M. Allan, I.I. Fabrikant, Adv. At. Mol. Opt. **49**, 85 (2003)
2. R. Balog, J. Langer, S. Gohlke, M. Stano, H. Abdoul-Carime, E. Illenberger, Int. J. Mass. Spectrom. **233**, 267 (2004)
3. L. Sanche, Eur. Phys. J. D **35**, 367 (2005)
4. J.W. McConkey, C.P. Malone, P.V. Johnson, C. Winstead, V. McKoy, I. Kanik, Phys. Rep. **466**, 1 (2008)
5. I. Baccarelli, I. Bald, F.A. Gianturco, E. Illenberger, J. Kopyra, Phys. Rep. **508**, 1 (2011)
6. J.M. Rice, G.O. Dudek, M. Barber, J. Am. Chem. Soc. **87**, 4569 (1965)
7. J. Ulrich, R. Teoule, R. Massot, A. Cornu, Org. Mass Spectrom. **2**, 1183 (1969)
8. M. Imhoff, Z. Deng, M.A. Huels, Int. J. Mass Spectrom. **245**, 68 (2005)
9. R. Abouaf, J. Pommier, H. Dunet, Chem. Phys. Lett. **381**, 486 (2003)
10. C. Dal Cappello, I. Charpentier, S. Houamer, P.A. Hervieux, M.F. Ruiz-Lopez, A. Mansouri, A.C. Roy, J. Phys. B **45**, 175205 (2012)
11. C. Dal Cappello, Z. Rezkallah, S. Houamer, I. Charpentier, A.C. Roy, P.A. Hervieux, M.F. Ruiz-Lopez, Eur. Phys. J. D **67**, 117 (2013)
12. M.A. Huels, I. Hahndorf, E. Illenberger, L. Sanche J. Chem. Phys. **108**, 1309 (1998)
13. S. Denifl, S. Ptasińska, M. Cingel, S. Matejcik, P. Scheier, T.D. Märk, Chem. Phys. Lett. **377**, 47 (2003)
14. S. Denifl, S. Ptasińska, M. Probst, J. Hrušák, P. Scheier, T.D. Märk, J. Phys. Chem. A **108**, 6562 (2004)
15. R. Abouaf, H. Dunet, Eur. Phys. J. D **35**, 405 (2005)
16. H. Abdoul-Carime, S. Gohlke, E. Illenberger, Phys. Rev. Lett. **92**, 168103 (2004)
17. S. Ptasińska, S. Denifl, V. Grill, T.D. Märk, P. Scheier, S. Gohlke, M.A. Huels, E. Illenberger, Angew. Chem. Int. Ed. **44**, 1647 (2005)
18. S. Ptasińska, S. Denifl, P.L. Scheier, E. Illenberger, T.D. Märk, Angew. Chem. Int. Ed. **44**, 6941 (2005)
19. S. Ptasińska, S. Denifl, B. Mróz, M. Probst, V. Grill, E. Illenberger, P. Scheier, T.D. Märk, J. Chem. Phys. **123**, 124302 (2005)
20. F. Ferreira da Silva, C. Matias, D. Almeida, G. García, O. Ingólfsson, H.D. Flosadóttir, B. Ómarsson, S. Ptasinska, B. Puschnigg, P. Scheier, P. Limão-Vieira, S. Denifl, J. Am. Soc. Mass Spectrom. **24**, 1787 (2013)
21. D. Almeida, D. Kinzel, F. Ferreira da Silva, B. Puschnigg, D. Gschliesser, P. Scheier, S. Denifl, G. García, L. González, P. Limão-Vieira, Phys. Chem. Chem. Phys. **15**, 11431 (2013)
22. P.D. Burrow, G.A. Gallup, A.M. Scheer, S. Denifl, S. Ptasinska, T. Märk, P. Scheier, J. Chem. Phys. **124**, 124310 (2006)
23. X. Li, M.D. Sevilla, L. Sanche, J. Phys. Chem. B **108**, 19013 (2004)
24. A. Dora, L. Bryjko, T. van Mourik, J. Tennyson, J. Phys. B **45**, 175203 (2012)
25. R. Improta, G. Scalmani, V. Barone, Int. J. Mass Spectrom. **201**, 321 (2000)
26. H.-W. Jochims, M. Schwell, H. Baumgärtel, S. Leach, Chem. Phys. **314**, 263 (2005)
27. E. Itälä, D.T. Ha, K. Kooser, E. Rachlew, M.A. Huels, E. Kukk, J. Chem. Phys. **133**, 154316 (2010)
28. J. de Vries, R. Hoekstra, R. Morgenstern, T. Schlathölter, Eur. Phys. J. D **24**, 161 (2003)
29. J. de Vries, R. Hoekstra, R. Morgenstern, T. Schlathölter, Phys. Rev. Lett. **91**, 053401 (2003)
30. J. de Vries, R. Hoekstra, R. Morgenstern, T. Schlathölter, Phys. Scr. **T110**, 336 (2004)

31. T. Schlathölter, R. Hoekstra, R. Morgenstern, Int. J. Mass Spectrom. **233**, 173 (2004)
32. T. Schlathölter, F. Alvarado, R. Hoekstra, Nucl. Instrum. Methods Phys. Res. B **233**, 62 (2005)
33. J. Tabet, S. Eden, S. Feil, H. Abdoul-Carime, B. Farizon, M. Farizon, S. Ouaskit, T.D. Märk, Int. J. Mass Spectrom. **292**, 53 (2010)
34. S.K. Kim, W. Lee, D.R. Herschbach, J. Phys. Chem. **100**, 7933 (1996)
35. N.J. Kim, H. Kang, G. Jeong, Y.S. Kim, K.T. Lee, S.K. Kim, J. Chem. Phys. **115**, 15 (2001)
36. T. Kagawa, K. Aikawa, F. Sato, Y. Kato, T. Iida, Radiat. Prot. Dosim. **122**, 95 (2006)
37. T. Schlathölter, F. Alvarado, S. Bari, A. Lecointre, R. Hoekstra, V. Bernigaud, B. Manil, J. Rangama, B. Huber, ChemPhysChem **7**, 2339 (2006)
38. F. Zappa, S. Denifl, I. Mähr, J. Lecointre, F. Rondino, O. Echt, T.D. Märk, P. Scheier, Eur. Phys. J. D **43**, 117 (2007)
39. G. Barrett, P.J.M. van der Burgt, J. Phys.: Conf. Ser. **101**, 012008 (2008)
40. Y. Itikawa, N. Mason, J. Phys. Chem. Ref. Data **34**, 1 (2005)
41. S. Denifl, B. Sonnweber, G. Hanel, P. Scheier, T.D. Märk, Int. J. Mass Spectrom. **238**, 47 (2004)
42. I.I. Shafranyosh, M.I. Sukhoviya, M.I. Shafranyosh, L.L. Shimon, Tech. Phys. **53**, 1536 (2008)
43. Ph. Bernhardt, H.G. Paretzke, Int. J. Mass Spectrom. **223-224**, 599 (2003)
44. P. Możejko, L. Sanche, Radiat. Environ. Biophys. **42**, 201 (2003)
45. C. Champion, J. Chem. Phys. **138**, 184306 (2013)
46. M. Vinodkumar, Ch. Limbachiya, M. Barot, M. Swadia, A. Barot, J. Mass Spectrom. **339-340**, 16 (2013)
47. W.M. Huo, C.E. Dateo, G.D. Fletcher, NASA Technical Report NAS-06-009, 2006
48. A. Peudon, S. Edel, M. Terrissol, Radiat. Prot. Dosim. **122**, 128 (2006)
49. P.J.M. van der Burgt, Eur. Phys. J. D **68**, 135 (2014)
50. J.-C. Fan, Z.-C. Shang, J. Liang, X.-H. Liu, H. Jin, J. Mol. Struct. (Theochem) **939**, 106 (2010)
51. A.B. Trofimov, J. Schirmer, V.B. Kobychev, A.W. Potts, D.M.P. Holland, L. Karlsson, J. Phys. B **39**, 305 (2006)
52. J. González-Vázquez, L. González, E. Samoylova, T. Schultz, Phys. Chem. Chem. Phys. **11**, 3927 (2009)